JOURNAL OF CATALYSIS **168,** 301–314 (1997)
ARTICLE NO. CA971683

Selective Hydrogenation of Cinnamaldehyde over Supported Copper Catalysts

Alan Chambers,* S. David Jackson,† Diane Stirling,‡,[1] and Geoffrey Webb‡

*Chemistry Department, University of Wales, Cardiff CF1 3TB, United Kingdom; †ICI Katalco, Research and Technology Centre, Billingham TS23 1LB, United Kingdom; and ‡Chemistry Department, University of Glasgow, Glasgow G12 8QQ, United Kingdom

Received May 23, 1996; revised January 22, 1997; accepted February 28, 1997

The selective hydrogenation of cinnamaldehyde in the liquid phase has been studied using silica-supported catalysts. Selectivity to cinnamyl alcohol was found to be dependent on both the silica used and the way in which the catalyst had been prepared. The highest selectivity was achieved using a 13.7 wt% Cu/PQ-silica catalyst prepared by an impregnation route. This catalyst contained large copper crystallites and small amounts of Cu_2O at the metal–support interface. Modification of the catalyst by doping with palladium resulted in an acceleration of the rate of reaction but a loss in selectivity. CuO/V_2O_5/PQ-silica formed a copper-vanadia bronze on reduction, but the rate of hydrogenation of cinnamaldehyde was much lower than for Cu/PQ-silica and the catalyst was not selective for cinnamyl alcohol. The hydrogenation of cinnamaldehyde over the supported copper catalysts proceeded on a modified surface formed from adsorbed hydrocinnamaldehyde. Cinnamaldehyde was hydrogenated to hydrocinnamaldehyde and, in some cases, also cinnamyl alcohol. Hydrocinnamaldehyde was then further hydrogenated to phenyl propanol. Selectivity to cinnamyl alcohol using the 13.7 wt% Cu/PQ silica catalyst remained high even at 80% conversion.

INTRODUCTION

The selective hydrogenation of α,β-unsaturated carbonyl compounds to their corresponding unsaturated alcohols is an important step in the preparation of various fine chemicals such as fragrances for the perfume industry (1). The hydrogenation of unsaturated carbonyl compounds has been studied using copper-chromite catalysts (2–4), since copper has been shown to preferentially hydrogenate the carbonyl group (2) unlike platinum which favours hydrogenation of the unsaturated carbon atoms (5). However, although good selectivity to unsaturated alcohols was achieved using the copper–chromite catalyst for the hydrogenation of nonconjugated systems, surprisingly low selectivity was obtained in the hydrogenation of α,β-unsaturated aldehydes or ketones (2). The reaction mechanism is unclear, but allylic alcohols are strongly adsorbed on the catalyst surface and may undergo isomerisation to the aldehyde under the influence of the chromia support which is known to catalyse isomerisation reactions (3).

Supported iridium (6), ruthenium (7), cobalt (8), osmium (9), and platinum (10) catalysts have been investigated for their selectivity to cinnamyl alcohol in the hydrogenation of cinnamaldehyde. Selectivity to cinnamyl alcohol is governed by the presence of promoters, metal particle size, and the nature of the support. Thus, supported platinum catalysts have been found to give poor selectivity to unsaturated alcohols, but high selectivity can be induced by the addition of small amounts of metal chlorides such as $FeCl_2$ (11). The more electropositive iron increases the electron density on platinum, lowering the probability of C=C activation and polarising the C=O for nucleophilic attack on the carbon atom by hydrogen dissociated on neighboring platinum atoms. Promotion of platinum on silica by tin has been found to increase selectivity to the allyl alcohol in the hydrogenation of acrolein (12), and selectivity to cinnamyl alcohol in the hydrogenation of cinnamaldehyde was also improved when $SnCl_2$ was added to supported ruthenium catalysts (13). Galvagno *et al.* (11) stressed that such promotional effects could not be due to the presence of chlorine, but Nitta *et al.* (8) found that higher selectivities to cinnamyl alcohol were obtained for the hydrogenation of cinnamaldehyde over cobalt on silica catalysts when they were prepared from chloride rather than nitrate precursors. This was attributed both to chloride aiding the reduction of the supported precursor and thus creating a more uniform particle size distribution, and the surface chloride remaining after reduction depressing the hydrogenation of C=C. Particle size effects have been demonstrated for the hydrogenation of cinnamaldehyde using supported ruthenium (7), platinum (10), and cobalt (14) catalysts. Larger particles were found to give higher selectivity to cinnamyl alcohol in each case. This has been attributed to steric effects (7), where the phenyl group prevents the close approach of the C=C to the surface of a large particle so that the molecule

[1] To whom correspondence should be addressed. E-mail: D.Stirling @chem.gla.ac.uk.

0021-9517/97 $25.00

is tilted with C=O closer to the surface and therefore more easily activated. There is no such barrier to the approach of the phenyl group to a small particle and, therefore, the selectivity to cinnamyl alcohol is low. The influence of the support on selectivity in the hydrogenation of cinnamaldehyde has been demonstrated using supported platinum and ruthenium catalysts. Higher selectivities to cinnamyl alcohol were observed when either platinum or ruthenium were supported on graphite rather than charcoal (6).

In this paper we report on a study of the hydrogenation of cinnamaldehyde using modified silica-supported copper catalysts. Our aim was to achieve a better understanding of the factors influencing activity and selectivity. Silica was chosen as the support to exploit the preferential C=O hydrogenation activity of copper without inducing isomerisation of the resultant allyl alcohols as observed for the copper–chromite catalysts. Palladium was chosen as a modifier for the supported copper catalysts on account of its high activity for the hydrogenation of aromatic aldehydes (9) and its ability to dissociate and absorb hydrogen. $Cu/V_2O_5/SiO_2$ catalysts were also prepared since V_2O_5 can be reduced to a mixed valence metal oxide bronze (15) which would provide a mechanism for storing and releasing hydrogen and therefore have the potential to control selectivity.

EXPERIMENTAL

1. *Catalyst Preparation*

The supported copper and modified supported copper catalysts were prepared by impregnation of industrially supplied pelletised silicas with appropriate concentrations of metal salt solutions. Excess liquid was used in the impregnation step, and excess water was removed using a rotary evaporator unless stated otherwise. Two pelletised silicas were used, namely PQ silica (PQ Corporation, USA) with a surface area of 200 $m^2\ g^{-1}$ and a mean pore diameter of 20 nm and Grace silica (Fuji Silysia Chemical Limited, Japan) which had a surface area of 280 $m^2\ g^{-1}$ and a mean pore diameter of 10 nm. The PQ silica was comprised of cylindrical pellets 5 mm long and 1 mm diameter. The Grace silica was comprised of 3 mm diameter spheres. The following catalyst precursors were prepared on PQ silica.

Cu/PQ silica. PQ silica was impregnated with sufficient $Cu(NO_3)_2 \cdot 3H_2O$ (aq) to give loadings of 13.7 wt% Cu (CuA/PQ), 12.4 wt% Cu (CuB/PQ), or 6.1 wt% Cu (CuC/PQ).

CuA/Pd/PQ. Samples of impregnated and dried CuA/PQ were impregnated with $Pd(NO_3)_2$ (aq) to give Pd concentrations of 100 ppm (CuA/Pd1/PQ), 790 ppm (CuA/Pd2/PQ), and 1500 ppm (CuA/Pd3/PQ). A further sample of impregnated and dried CuA/PQ was impregnated with $PdCl_2$ (aq) to give a palladium concentration of 100 ppm (CuA/Pd4/PQ).

V/PQ. PQ silica was impregnated with sufficient NH_4VO_3 (aq) to give a 9.3 wt% loading of V_2O_5. In this case, the silica was dipped in the NH_4VO_3 solution for 30 min and then drained prior to oven drying.

CuB/V/PQ. $Cu(NO_3)_2 \cdot 3H_2O$ (aq) was impregnated onto dried (393 K) and calcined (723 K) V/PQ to give loadings of 12.1 wt% Cu and 7.8 wt% V_2O_5.

CuB/Pd/V/PQ. Solutions of $Cu(NO_3)_2 \cdot 3H_2O$ (aq) and $Pd(NO_3)_2$ (aq) were separately impregnated onto V/PQ, excess water being removed on a rotary evaporator between impregnations, giving loadings of 12.6 wt% Cu, 7.6 wt% V_2O_5, and 220 ppm Pd.

Cu/Grace silica. Supported copper catalyst precursors were also prepared on Grace silica. Grace silica was impregnated with sufficient $Cu(NO_3)_2 \cdot 3H_2O$ (aq) to give Cu loadings of 12.4 wt% (CuA/Grace) and 5.6 wt% (CuB/Grace).

All the impregnated catalysts described above were oven dried at 393 K and calcined at 723 K for 3 h in a muffle oven. In addition to this, some dried samples of CuA/PQ were calcined in flowing air at either 623 K (CuAFL623/PQ) or 723 K (CuAFL723/PQ). The impregnated and dried precursors will be denoted in the text as CuA/PQ, CuB/PQ, etc., as listed above. The prefixes "cal" or "red" will be added when referring to the calcined or calcined and reduced samples, respectively. Catalysts CuB/PQ, CuC/PQ, V/PQ, CuB/V/PQ, CuB/V/Pd/PQ, CuA/Grace, and CuB/Grace were all prepared in an industrial laboratory using an AnalaR quality $Cu(NO_3)_2 3H_2O$ salt manufactured at ICI C & P Ltd. Catalysts CuA/PQ and CuA/Pd/PQ were prepared at Glasgow using AnalaR grade $Cu(NO_3)_2 3H_2O$ supplied by Aldrich. All the other salts used in these preparations were of AnalaR quality. Metal loadings were determined for the calcined samples using atomic absorption spectroscopy. The copper, palladium, and V_2O_5 loadings for each of the calcined precursors are detailed in the above section.

2. *Characterisation of the Supported Oxides*

(a) Catalyst texture. BET surface areas (N_2, 77 K) were obtained from five-point adsorption isotherms using a Flowsorb 2300 Micromeritics instrument. The porosities of the supports and the calcined catalyst precursors were determined by mercury porosimetry using an Autopore 9220.

(b) Temperature programmed reduction (TPR). The reducibility of the silica-supported transition metal oxides was assessed by temperature programmed reduction using an apparatus similar to that described by Robertson *et al.* (16) in which the temperature of the supported oxide catalyst precursor was increased linearly at 10 K min^{-1} in 6% H_2/N_2 at a flow rate of 40 $cm^3\ min^{-1}$. Generally, the temperature was increased from ambient to 873 K, but for catalysts containing palladium the experiments were begun at 193 K since some palladium salts reduce at or below

room temperature. A thermal conductivity detector was used to measure changes in hydrogen concentration in the gas stream resulting from the uptake of hydrogen by the catalyst. The detector was calibrated by injecting known amounts of hydrogen into a stream of nitrogen.

(c) Hot stage x-ray powder diffraction (XRD). Hot stage XRD studies of the calcined catalyst precursors calCuA/PQ, calCuB/PQ, calCuA/Grace, calV/PQ, calCuB/V/PQ, calCuA/Pd1/PQ, and calCuB/Pd/V/PQ were carried out using a Siemens Kristalloflex D500 diffractometer and Ni-filtered Cu-Kα radiation ($\lambda = 0.1542$ nm). Catalysts were heated in 1.5% H_2 in N_2 from 303 K to 423 K and then in 50 K steps up to 573 K. A diffraction trace was collected at each temperature step.

3. Characterisation of the Reduced Supported Oxides

(a) Chemisorption studies. The copper metal surface areas of the reduced supported oxides were determined using N_2O decomposition. The supported oxides were reduced in 6% H_2 in N_2 at 623 K, cooled in helium, and then 10 μl pulses of N_2O were passed over the catalysts at 333 K. N_2O underwent decomposition at the copper surface sites (17) and the evolved N_2 was separated chromatographically and detected by a thermal conductivity detector to give a direct measure of the copper surface area.

(b) Electron microscopy. The calcined catalyst precursors calCuA/PQ and calCuB/PQ were examined on a JEOL 1200 EX transmission electron microscope after reduction in 6% H_2 in N_2 at 673 K. Specimens were prepared by suspending them in water and then mounting them on carbon-filmed copper grids.

4. Catalytic Testing

The liquid phase hydrogenation of cinnamaldehyde in decalin was carried out in a glass reactor. A known weight of the calcined precursor to the catalyst ($\sim$0.3 g) was placed in the bottom of the reactor and the reactor was inverted so that the catalyst was evenly distributed over a porous sinter. The sinter was surrounded by a furnace. The apparatus was flushed with helium at room temperature. The gas flow was then changed to 6% hydrogen in nitrogen and the temperature was ramped up to 673 K at 20 K min^{-1} and maintained at this temperature overnight. The reactor was then cooled to room temperature in helium and turned upright again; 25 ml of decalin followed by 250 μl of cinnamaldehyde were then injected through a rubber septum into the reactor and the reaction mixture was raised to a temperature of 413 K using an oil bath. Hydrogen was then passed through a bubbler inserted into one arm of the reactor into the mixture at a flow rate of 35 cm^3 min^{-1}. The hydrogen bubbler contained a porous sinter to disperse the hydrogen in the solvent more effectively. The reaction mixture was vigorously agitated throughout the catalytic run using a magnetic stirrer bar. The reaction mixture was maintained at 413 K during the catalysed reaction and a condenser was attached to the H_2 exit to prevent solvent loss. Aliquots of the reaction mixture were removed from the reaction vessel during the course of the reaction and analysed by gas chromatography using a 5% carbowax 20M on chromosorb W column and a flame ionisation detector.

5. Mechanistic Studies

The mechanism of the hydrogenation of cinnamaldehyde was followed by employing deuterium as a tracer. In these studies, deuterium was reacted with cinnamaldehyde instead of hydrogen. The calcined catalyst precursor (1.80 g calCuA/PQ) was reduced in hydrogen at 673 K as before using the reactor in its inverted position. The reactor was then turned upright and the catalyst was covered in 15 cm^3 of decalin. Deuterium was then bubbled through the solvent at 2 cm^3/min, 2 cm^3 of cinnamaldehyde was added to the reaction mixture, and the reaction was carried out at 408 K. The composition of the reaction mixture was measured during the course of the reaction by gas chromatography, as described previously. The reaction mixture was also analysed by proton and deuterium NMR using a Bruker AM 200 MHz spectrometer. Chloroform was used as the solvent for the NMR work.

RESULTS

1. Characterisation of the Supported Oxides

(a) Catalyst morphology. The BET surface areas and porosities for the silicas and the calcined catalyst precursors are given in Table 1. The lower surface area silica, PQ, had a bimodal pore size distribution with the majority of the pores $\sim$20 nm, and $\sim$10% of the pores $\sim$100 nm in diameter. All the pores in Grace silica were concentrated in a narrow band $\sim$10 nm in diameter. The results show that impregnating either PQ or Grace silica with either $Cu(NO_3)_2 \cdot 3H_2O$ (aq) or NH_4VO_3 (aq) and decomposition to the supported oxides resulted in a similar loss in surface area and corresponding decrease in mean pore diameter. A further loss in area occurred on impregnating and calcining PQ silica with both salts. No further loss in surface area occurred on adding $Pd(NO_3)_2$ to PQ silica.

(b) Hot stage XRD. The calcined catalyst precursors were initially examined in the diffractometer at room temperature to identify the phases present. Amorphous silica was identified in all the samples as the major phase, giving a broad peak with a d spacing of 0.41 nm in each case. CuO (tenorite structure) was found in all the copper-containing catalysts. The vanadium-containing catalysts all contained V_2O_5. Palladium was present at concentrations of $\leq$220 ppm in the two palladium-doped catalysts studied by XRD, i.e., calCuA/Pd1/PQ and calCuB/Pd/V/PQ, so

TABLE 1

BET Surface Areas and Mercury Porosimetry Data for the Silicas and the Calcined Catalyst Precursors

Silica or catalyst precursor	N_2 surface area ($m^2\ g^{-1}$)	Average pore diameter (nm)	Total intrusion volume ($cm^3\ g^{-1}$)	Total pore area ($m^2\ g^{-1}$)
PQ silica	200	20	[a]	[a]
CuA/PQ	182	18	1.02	228
CuB/PQ	165	19	1.03	216
V/PQ	169	18	0.97	215
CuB/V/PQ	135	17	0.83	187
CuB/Pd/V/PQ	138	17	0.80	190
Grace silica	280	10	[a]	[a]
CuA/Grace	243	10	0.84	324

[a] Data not available.

no characteristic phase was identified for PdO. A further unidentified phase was found, however, in catalysts containing copper and vanadium. This may be indicative of interaction between the copper and the vanadium oxide rather than V_2O_5 interacting with the silica, since the phase was not found to be present for V_2O_5/PQ.

The diffraction patterns for the three CuO-on-silica samples studied, namely calCuA/PQ, calCuB/PQ, and calCuA/Grace, were quite similar, but the CuO was more crystalline and gave a more intense pattern for both calCuB/PQ and calCuA/Grace, compared with calCuA/PQ. After an initial examination in the diffractometer, the samples were heated from 303 K to 673 K in 4% H_2 in N_2. Data were collected at 25 K intervals between 323 K and 673 K with a final scan after cooling to 303 K. The sequence of diffraction patterns for the three CuO-on-silica samples around the phase changes from CuO to Cu_2O and/or Cu are shown in Fig. 1. Before reduction, all three samples showed diffraction patterns characteristic of CuO tenorite, with peaks at $2\theta = 35.6$, 38.8, 38.9, 46.3, 48.6, and 53.5°. Reduction of the tenorite to copper metal commenced at 473 K on calCuA/Grace (Fig. 1A). This was indicated by the appearance of the copper(111) and copper(200) diffraction peaks at $2\theta = 43.3$ and 50.4°, respectively. The copper phase component in the diffraction pattern increased relative to the tenorite as the temperature was increased further and the last traces of tenorite had disappeared completely by 548 K. Similarly, calCuB/PQ underwent a tenorite to copper phase change, but copper metal was not observed until 498 K (Fig. 1B) Traces of tenorite were still observed at 523 K as was the case for calCuA/Grace, but, they had disappeared completely by 548 K. There was no evidence for the formation of Cu_2O in either the CuA/Grace or CuB/PQ catalysts. CalCuA/PQ behaved quite differently, however, with Cu_2O (cuprite) being formed as an intermediate in the reduction of tenorite to copper. Cuprite and a trace of copper were observed at 523 K with tenorite still present as the major phase (Fig. 1C). The presence of the cuprite was indicated by the appearance of the Cu_2O (111) diffraction peak at $2\theta = 36.4°$. Cuprite was still present at 548 K, but it had virtually disappeared by 573 K. Tenorite was still present as a trace phase even at 648 K, indicating that calCuA/PQ was much more difficult to reduce than either calCuB/PQ or calCuA/Grace.

CalV/PQ did not undergo any change during the reduction experiment. The observed traces for the reduction of CuO in calCuB/V/PQ were very similar to those of calCuB/PQ with copper metal first appearing at 498 K and the reduction being complete at 548 K. However, the unidentified phase present in the unreduced sample began to change at 498 K and had disappeared by 523 K. The reduction temperature of CuO on PQ silica was lowered in the presence of palladium. Thus CuO in calCuB/Pd/PQ reduced directly to copper, with copper being first observed at 448 K and reduction being complete by 498 K. Palladium had a similar although less marked effect on the reduction temperature in calCuB/Pd/V/PQ, with the CuO being reduced between 498 and 523 K. The unidentified phase present in unreduced calCuB/Pd/V/PQ became less well defined at 473 K and had completely disappeared by 498 K.

Crystallite size measurements were obtained for each of the main crystalline phases observed in the samples described above. The tenorite(002), copper(111), and cuprite(111) diffraction peaks were selected for this work. A simple Scherrer equation interpretation of the full-width half-maximum corrected for the intrinsic instrument broadening was used to determine the crystallite sizes from the diffraction peaks (18). It was assumed that sample-dependent broadening was due to crystallite size effects rather than lattice distortions. Crystallite sizes were measured at 25 K intervals over the temperature range 298 to 673 K. The tenorite phase in unreduced calCuA/Grace was found to have a crystallite size of ~18 nm and disappeared abruptly once the copper phase with a crystallite size of ~17 nm formed on reduction. There was little change in the copper crystallite size over the temperature range and reduction time studied, indicating that sintering of the phases did not occur. Sintering of the tenorite occurred in calCuB/PQ above 523 K, where the copper phase first appeared, and particles as large as 55 nm were observed at 623 K. However, the copper crystallites in calCuB/PQ did not sinter and had a crystallite size of ~21 nm. Sintering of the copper phase did occur in calCuA/PQ in which the reduction process was much slower and a cuprite intermediate was detected. Copper crystallites were formed with a particle size of 30 nm after reduction at 673 K. Table 2 lists the crystallite sizes for the three supported copper catalysts, calCuB/Pd/PQ, calCuB/V/PQ, and calCuB/V/Pd/PQ, studied at the "crossover point." This is the temperature at which the tenorite and copper phases were present in equal amounts. There was no evidence of

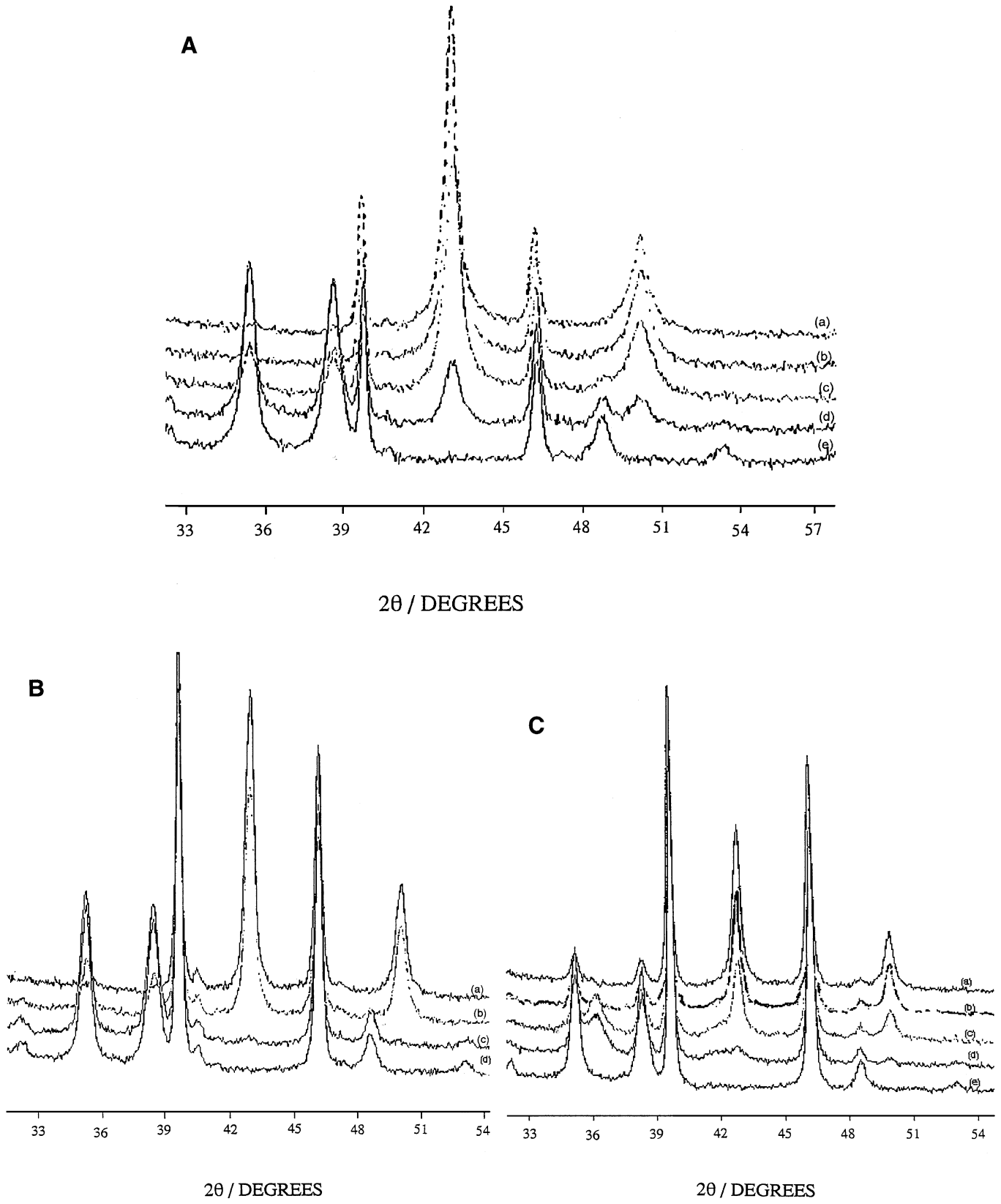

FIG. 1. X-ray diffraction patterns for: (A) calCuA/Grace after reduction at (a) 548 K, (b) 523 K, (c) 498 K, (d) 473 K, (e) 448 K; (B) calCuB/PQ after reduction at (a) 523 K, (b) 498 K, (c) 473 K, (d) 448 K, (C) calCuA/PQ after reduction at (a) 598 K, (b) 573 K, (c) 548 K, (d) 523 K, (e) 498 K.

TABLE 2

Crystallite Sizes for the Supported Copper and Modified Supported Copper Catalysts at the "Crossover Point"

Catalyst	"Crossover" temp. of reduction (K)	Crystallite size tenorite (nm)	Crystallite size copper (nm)
CuA/Grace	483	18.0	17.0
CuA/PQ	543	23.5–25.0	11.0–31.5
CuA/Pd/PQ	473	21.0	16.5
CuB/PQ	508	19.0	21.0
CuB/V/PQ	508	21.0	21.0–23.5
CuB/Pd/V/PQ	473	23.5–25.0	26.0

sintering for calCuB/Pd/PQ during reduction, and the copper crystallites at the "crossover point" were much smaller than for calCuB/PQ. Although palladium was not detected as a separate phase, it is readily reducible (19) and may provide a source of hydrogen for the reduction of tenorite which occurred at a lower temperature in the presence of palladium. The smaller copper crystallite size probably reflects the milder reduction conditions in the presence of palladium and shows that the particles did not sinter once formed. Vanadia had little effect on the reduction of CuO in calCuB/V/PQ except that, unlike calCuB/PQ, no sintering of the tenorite occurred as the reduction temperature was increased. The reduction temperature of CuO was lowered on adding palladium to calCuB/V/PQ, but there was an increase in the size of the copper crystallites.

(c) Temperature programmed reduction (TPR). The calcined catalyst precursors, together with unsupported CuO and $Cu(NO_3)_2 3H_2O$ that had been calcined at 713 K for 3 h, were all characterised by TPR using the standard conditions described in the Experimental section. The temperature at each peak maximum, the measured hydrogen consumption per gram of catalyst and the theoretical hydrogen consumption for each calcined catalyst precursor are given in Table 3.

The TPR profile for AnalaR grade CuO consisted of a single reduction peak at 553 K corresponding to the complete reduction of CuO to Cu. Calcined $Cu(NO_3)_2 \cdot 3H_2O$ was also reduced in one step to Cu, but the peak maximum was shifted to 653 K. The reduction of unsupported CuO has been studied by a number of authors (16, 19, 20). Reduction always occurred in a single step corresponding to the complete reduction of CuO to Cu. The temperature of the peak maximum in the reduction profile was dependent on the origin and pretreatment of the sample, the hydrogen concentration in the reduction gas, gas flow rate, heating rate, and sample size. It is thus important to examine the reduction characteristics of the unsupported oxide under the operating conditions of the experimental system used for the TPR studies. Since the operating conditions were kept constant for CuO and calcined $Cu(NO_3)_2 \cdot 3H_2O$, the variation in reduction temperatures can be attributed to variations in the particle size of the CuO from the two sources. Similar effects have been observed previously. Thus AnalaR CuO was observed to reduce with a peak maximum at 553 K using 5% H_2/N_2 at a flow rate of 48 cm^3 min^{-1} and a heating rate of 12 K min^{-1} (20), and CuO obtained by nitrate calcination yielded a reduction maximum at 640 K using 6% H_2/N_2 at a flow rate of 10 cm^3 min^{-1} and a heating rate of 6.5 K min^{-1} (16). It is likely that decomposition of unsupported $Cu(NO_3)_2 \cdot 3H_2O$ at 723 K will have resulted in some sintering to give large CuO particles which would be more difficult to reduce.

The TPR profiles for calCuA/Grace and calCuB/Grace resembled the profile obtained for unsupported CuO, reduction occurring in a single step and corresponding to the complete reduction of CuO to Cu. This was in agreement with the hot stage XRD results reported for calCuA/Grace which showed no evidence for the intermediate formation of Cu_2O and complete reduction to copper by 548 K. The TPR at 563 and 546 K for calCuA/Grace and calCuB/Grace, respectively, are at lower temperatures than the profiles for unsupported CuO prepared from nitrate calcination. The silica therefore appears to simply act as a support medium for the stabilisation of small, highly dispersed copper particles. The lower reduction temperature for calCuB/Grace, compared with calCuA/Grace, is consistent with the results of Delk and Vavere (21), who showed that a decrease in the copper content of silica-supported catalysts led to a decrease in the reduction temperature. A higher reduction

TABLE 3

Temperatures of Reduction Maxima and Hydrogen Consumption for the Calcined Catalyst Precursors and Copper Surface Areas for the Reduced Catalysts

Catalyst precursor	T max (K)	H_2 consumption (cm^3 g^{-1})		Copper surface area (m^2 g^{-1})[b]
		Experimental	Theoretical[a]	
CuA/PQ	608, 628	43.93 ± 6%	51.92	0.08
CuA/Pd1/PQ	263, 599	47.93 ± 6%	49.92	0.71
CuA/Pd2/PQ	263, 532	44.33 ± 5%	51.92	0.55
CuA/Pd3/PQ	263, 455, 543	45.92 ± 5%	64.30	0.67
CuA/Pd4/PQ	263, 697, 729	49.52 ± 12%	50.72	0.45
CuB/PQ	603	41.14 ± 9%	47.13	0.40
CuC/PQ	559	21.17 ± 11%	23.16	—
CuB/V/PQ	603	52.72 ± 10%	55.91	0.42
CuB/V/Pd/PQ	263, 613	57.51 ± 11%	57.51	0.57
V/PQ	613, 808, 893	7.59 ± 16%	11.98 ($V^V \rightarrow V^{IV}$)	—
CuA/Grace	563	44.73 ± 3%	47.13	2.18
CuB/Grace	546	16.38 ± 3%	16.77	0.53
CuA/PQ/CIA	568, 603	47.13 ± 5%	51.92	0.15
CuA/PQ/CIA 623 K	525, 578, 598	48.33 ± 7%	51.92	0.40

[a] Refers to $Cu^{II} \rightarrow Cu^0$ (and $Pd^{II} \rightarrow Pd^0$) unless otherwise stated.
[b] Refers to Cu surface area (m^2 g^{-1} of catalyst).

temperature can be expected with higher copper content, since reduction is controlled by the rate of diffusion of hydrogen through the CuO particles (22).

The reducibility of CuO is not only dependent on sample pretreatment but also the nature of the silica support employed. Thus the reduction profiles obtained for CuO/PQ were much broader than those for CuO/Grace silica and shifted to higher temperatures. Furthermore, the data in Table 3 show that there is a marked discrepancy between the experimental and theoretical hydrogen consumptions for the CuO/PQ catalysts. Better agreement between the experimental and theoretical values was obtained for CuO/Grace. This indicated that a small amount of the CuO interacted strongly with the silica support and could not be reduced under the conditions studied. This is in agreement with the hot stage XRD results for calCuA/PQ which showed that a small amount of irreducible tenorite was detected even after reduction at 648 K. One broad peak centred at 559 K was detected in the TPR profile for calCuC/PQ (6.1% Cu loading). A high temperature shoulder at 620 K was observed in addition to the main peak at 603 K when the copper loading was increased to 12.4% (calCuB/PQ). It is unlikely that the peak and high temperature shoulder could be assigned to CuO in small and large pores, respectively, since on further increasing the loading to 13.7% Cu (CuA/PQ) two peak maxima at 608 and 628 K were observed in equal ratios. However, the broadening of the peaks on PQ, compared with Grace silica, suggests that the bimodal nature of the PQ silica influences the reduction profile. The two peaks in the reduction profile can be assigned to particle size effects and/or metal–support interactions. Copper crystallite sizes determined by X-ray line broadening studies showed that redCuA/PQ contained copper crystallites ranging in size from 11 to 31.5 nm, whereas all the particles were ~21 nm in redCuB/PQ. The two TPR peaks observed for calCuA/PQ and calCuB/PQ may, therefore, be due to the reduction of CuO particles of different sizes on the support. However, the consistently lower experimental hydrogen consumptions, compared with the expected uptake for the copper loading, suggests that this is not the entire explanation. It is likely that there is also some metal–support interaction, possibly stabilising small amounts of Cu_2O at the metal–support interface following reduction. The detection of Cu_2O as an intermediate lends weight to this explanation.

The observed TPR profile for calCuA/PQ was found to be dependent on the way in which the precursor was calcined. Calcination of the impregnated precursor at 723 K in flowing air, instead of using a muffle oven resulted in the reduction profile being shifted to lower temperatures. The reduction profile was shifted to even lower temperatures and an additional peak emerged at 525 K after calcination in flowing air at 623 rather than 723 K. The addition of 200–5000 ppm $Pd(NO_3)_2$ to the uncalcined CuA/PQ precursor followed by calcination in flowing air at 723 K caused a lowering in the temperature of the reduction maxima. A separate peak emerged at the highest loading. However, it was suspected that any PdO formed during the calcination step would be reduced at room temperature in 6% H_2/N_2. Further TPR runs were therefore carried out on all the palladium-containing catalysts in which the temperature program was run from 193 to 873 K. In each case, a small broad peak was detected at 263 K corresponding to the reduction of Pd(II) to Pd(0), in addition to the higher temperature peaks observed previously. The lowering of the reduction temperature of CuO in the presence of palladium indicates that the palladium may provide dissociated hydrogen for the facile reduction of CuO. The TPR profile for the calcined $PdCl_2$-doped CuA/PQ catalyst precursor (calCuA/Pd4/PQ) was very different from the $Pd(NO_3)_2$-doped catalyst precursors. CalCuA/Pd4/PQ contained additional peaks and was reduced at higher temperatures than its $Pd(NO_3)_2$-doped counterpart at the same Pd loading (calCuA/Pd1/PQ). It is likely that some of the chloride would be retained on calcination and that the additional peaks may therefore arise from the removal of chloride as HCl during reduction.

The TPR profile for the reduction of calV/PQ showed three distinct peaks at 613 K (5%), 808 K (30%), and 893 K (65%). These results are in broad agreement with those obtained by Roozeboom *et al.* (23). They studied the reduction of V_2O_5/SiO_2 prepared by an impregnation route. Two peaks were observed, namely a distinctive peak at 703 K and a second broader peak extending from 703 to 783 K. These peaks were assigned to surface and crystalline V_2O_5, respectively. The two-dimensional surface vanadate was predominantly in the form of VO_6 octahedra. On this basis, our observed peak at 613 K can be assigned to the surface vanadate and the peaks at 808 and 893 K to crystalline V_2O_5. The reduction of V_2O_5 in several stages has been reported previously (24, 25). Bosch *et al.* (24) concluded that the reduction proceeded as follows: $V_2O_5 \rightarrow \frac{1}{3}V_6O_{13} \rightarrow V_2O_3$. Other studies of supported V_2O_5 have indicated either reduction of V_2O_5 in a single step to V_2O_3 (26), or a two-stage reduction process, i.e., $V_2O_5 \rightarrow V_2O_4 \rightarrow V_2O_3$ (27). Thus the reducibility of the supported V_2O_5 is highly dependent on the preparative route, the nature of the support, and the conditions used for TPR. The observed hydrogen consumption for our sample, calV/PQ, is consistent with only partial reduction of V_2O_5 (observed H_2 consumption 7 $cm^3\ g^{-1}$, compared with 12 $cm^3 g^{-1}$ for $V_2O_5 \rightarrow V_2O_4$). However, the ability of V_2O_5 to absorb hydrogen and form bronzes casts some doubt on the validity of making any quantitative assessment of the hydrogen uptake for V/PQ.

The reduction profile for calCuB/V/PQ consisted of a single broad peak with a maximum at 603 K, i.e., the temperature recorded previously for the reduction of

calCuB/PQ. The hydrogen consumption corresponded to that required to reduce all the Cu(II) to Cu(0) with an oxidation state change of (I) for V_2O_5. No high temperature peaks were observed, the CuO and V_2O_5 therefore being reduced concomitantly. This result can be explained by hydrogen spillover, in which the hydrogen is reversibly adsorbed on the copper and then spills over onto the adjacent V_2O_5 causing it to be reduced. Similar spillover effects have been observed with $WO_3/Pt/Al_2O_3$ which forms tungsten bronzes (28). The TPR profile for calCuB/Pd/V/PQ was similar to that of calCuB/V/PQ over the temperature range 298 to 873 K, but low temperature studies starting at 193 K revealed an additional peak centred at 263 K corresponding to the reduction of all the Pd(II) to Pd(0), as was the case for calCuA/Pd/PQ.

2. Characterisation of the Reduced Supported Oxides

(a) Chemisorption studies. The copper metal surface areas of the reduced supported oxides area listed in Table 3. The copper surface area for the Grace-supported copper catalysts were higher than those for redCu/PQ, indicating that particle size effects played a dominant role in the poorer reducibility of the latter. The copper surface area decreased from 0.4 $m^2\ g^{-1}$ to 0.05 $m^2\ g^{-1}$ on increasing the Cu loading from 12.4 to 13.7% for redCu/PQ catalysts prepared under standard conditions, i.e., by calcination of the impregnated precursor salts at 723 K and reduction at 623 K. The copper surface area for redCuA/PQ increased to 0.4 $m^2\ g^{-1}$ when the calcination was carried out at 623 K in flowing air. The copper area only increased to 0.15 $m^2\ g^{-1}$ when the CuA/PQ-impregnated precursor was calcined in flowing air at 723 K, instead of in a muffle oven; this indicated that temperature rather than the method of calcination had the greatest effect on the copper surface area. The copper area for redCuA/PQ also increased in the presence of palladium in accordance with the TPR results. The copper surface area of the ex-chloride palladium-doped catalyst (redCuA/Pd4/PQ) was much lower than that for the ex-nitrate palladium-doped catalyst at the same loading (redCuA/Pd1/PQ). This may be attributed to residual chloride in redCuA/Pd4/PQ, providing a mechanism for the transport and subsequent aggregation of copper particle during reduction. The addition of V_2O_5 to CuB/PQ had no effect on the copper area, in accordance with the similarity in the TPR profiles for these samples. An increase in the copper area was observed on adding palladium to CuB/V/PQ.

(b) Electron microscopy. CuA/PQ and CuB/PQ were studied by transmission electron microscopy after calcination and reduction in H_2/N_2 in order to ascertain whether the observed differences in reducibility could be accounted for by differences in their particle morphologies or particle size distributions. RedCuB/PQ consisted of particles ranging from ~10 nm to ~250 nm. RedCuA/PQ contained less very small particles resulting in an overall increase in particle size. This is in accordance with the XRD results which indicated that redCuA/PQ contained a wider range of particle sizes than redCuB/PQ. Some large clusters of ~1000 nm were also observed in redCuA/PQ.

3. Catalytic Testing

Generally, 0.34 g of the calcined catalyst precursor was used in catalytic testing. Initially, however, catalyst weights ranging from 0.3 to 0.7 g were used to check that the reaction was not diffusion limited under the experimental conditions used. The rate constant was found to increase linearly with the amount of redCuA/PQ catalyst used, indicating the absence of external diffusion control under the conditions used.

The hydrogenation pathways for cinnamaldehyde hydrogenation are shown in Fig. 2. The bracketed 1-enol was never detected. However, a 1-enol is easily isomerised so the existence of a 1,4 process cannot be ruled out. The distribution of products (mole %) as a function of conversion is plotted for each catalyst in Figs. 3–7. In every case, the cinnamaldehyde concentration decreased linearly with respect to time except at very high conversions (80–90%). This indicates that the reaction is overall zero order at low and intermediate conversions. The deviations from linearity at high conversions presumably arise from there being insufficient cinnamaldehyde available at the surface to maintain the rate of reaction. The gradients of the linear regions of the plots of conversion against time were used to determine rate constants for each of the catalysts and are listed in Table 4. Table 4 also lists the percentage of hydrocinnamaldehyde and percentage of cinnamylalcohol and selectivity to cinnamyl alcohol at 60% conversion, where

$$\%\ \text{cinnamyl alcohol} = \frac{\text{mole fraction of cinnamyl alcohol}}{\text{mole fraction of cinnamaldehyde hydrogenated}} \times 100$$

$$\%\ \text{hydrocinnamaldehyde} = \frac{\text{mole fraction of hydrocinnamaldehyde}}{\text{mole fraction of cinnamaldehyde hydrogenated}} \times 100$$

$$\%\ \text{selectivity to cinnamyl alcohol} = \frac{\text{mole fraction of cinnamyl alcohol} \times 100}{\text{mole fraction of cinnamyl alcohol} + \text{hydrocinnamaldehyde}}.$$

For each catalyst studied, it was found that cinnamaldehyde was hydrogenated exclusively to hydrocinnamaldehyde during the initial stages of the reaction. This suggests

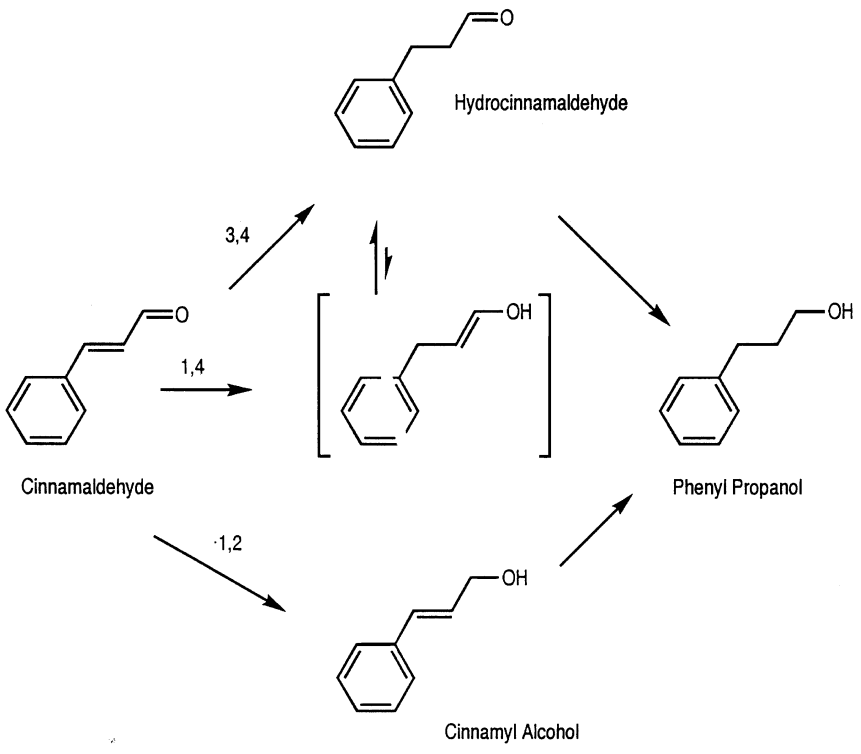

FIG. 2. Hydrogenation pathways for cinnamaldehyde hydrogenation.

that the catalyst surface is initially modified by hydrocinnamaldehyde, before further reaction to give cinnamyl alcohol and phenyl propanol can occur. A comparison of the plots of mole % against percentage conversion for the hydrogenation of cinnamaldehyde over the PQ silica-supported copper catalysts (Figs. 3–5) showed that reduced CuA/PQ gave a much higher selectivity to cinnamyl alcohol than reduced CuB/PQ or CuC/PQ. The selectivity decreased if the catalyst was calcined in flowing air, instead of in a muffle oven prior to reduction, and was completely lost if the catalyst was calcined at 623 K. Additional catalytic experiments were carried out using CuA/PQ that had been reduced at either 623 or 723 K, instead of the usual reduction of 673 K prior to the catalytic run. The activities and selectivities of these catalysts were the same as those for the catalyst after the standard reduction treatment. This shows that the overall rate of hydrogenation takes place preferentially on larger particles, which would be less affected by changes in the reduction conditions, and that catalyst selectivity is established prior to the reduction stage.

A comparison of the data in Tables 3 and 4 shows that the selective hydrogenation of cinnamaldehyde to cinnamyl alcohol occurs preferentially when little free copper is available, i.e., at sites associated with metal oxide–support interactions and/or on large particles. Thus reduced CuA/PQ was highly selective for cinnamyl alcohol, whereas CuB/PQ showed little selectivity to cinnamyl alcohol even though the overall rate of hydrogenation of cinnamaldehyde was the same for the two catalysts. The rate of hydrogenation of cinnamaldehyde on reduced CuC/PQ was lower, in accordance with its negligible copper surface area and TPR profile resembling that of bulk CuO, but it showed some selectivity towards cinnamyl alcohol (Table 4).

Addition of palladium to CuA/PQ increased the overall rate of hydrogenation of cinnamaldehyde markedly, but the selectivity to cinnamyl alcohol was lost (Fig. 6). The rate of hydrogenation of cinnamaldehyde for redCuA/Pd4/PQ (ex-chloride) was comparable to that of redCuA/Pd1/PQ, even though the copper area was substantially less,

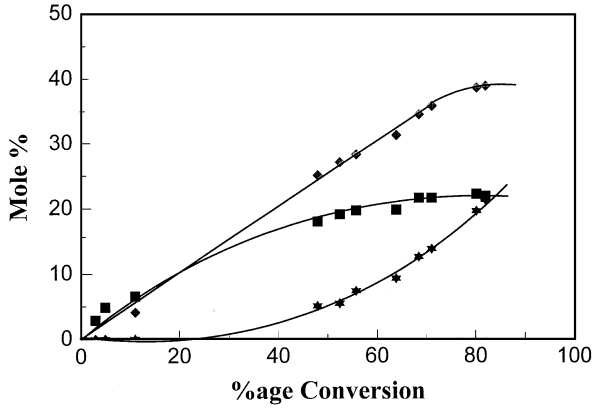

FIG. 3. Hydrogenation of cinnamaldehyde over reduced CuA/PQ: hydrocinnamaldehyde ■; cinnamyl alcohol ◆; phenyl propanol ★.

TABLE 4

Rate Constants, *k*, and Yields of Hydrocinnamaldehyde and Cinnamyl Alcohol at 60% Conversion

Catalyst	*k* (10^{-3} mol l^{-1} h^{-1})	% Yield hydrocinn. at 60% conv.	% Yield cinn. alcohol at 60% conv.	Time taken to reach 60% conv. (h)
RedCuA/PQ	1.5	33	48	32.75
RedCuB/PQ	1.5	55	2.5	24
RedCuC/PQ	0.6	46	27	71
RedCuA/Grace	3.3	67	5	14.5
RedCuB/Grace	3.1	78	8	15.3
RedCuB/V/PQ	0.6	[a]	[a]	[a]
RedCuB/V/Pd/PQ	7.1	71	5	6.8
RedCuA/Pd1/PQ	3.3	57	9	12.4
RedCuA/Pd2/PQ	6.1	57	—	6.6
RedCuA/Pd3/PQ	8.7	52	—	6.4
RedCuA/Pd4/PQ	3.3	60	13	11.2
RedCuA/PQ/CIA	2.1	38	39	23
RedCuA/PQ/CIA 623 K	2.7	83	—	17.6

[a] Very slow reaction.

suggesting that the chloride may be modifying the particle size rather than poisoning the catalyst.

"Reduced" V_2O_5/PQ was found to be inactive for the hydrogenation of cinnamaldehyde. The rate of hydrogenation of cinnamaldehyde using redCuB/V/PQ was much lower than that for redCuB/PQ, although both catalysts had the similar copper crystallite sizes and surface areas. RedCuB/V/PQ, like redCuB/PQ, was not selective for the 1,2 hydrogenation of cinnamaldehyde to cinnamyl alcohol. Addition of the palladium salt to the CuB/V/PQ precursor again increased the reaction rate for the reduced catalyst, but it had no effect on catalyst selectivity.

The rate of hydrogenation of cinnamaldehyde was much greater for redCuA/Grace (Fig. 7), compared with redCuB/PQ (similar loading), reflecting the higher copper surface areas attained on this support. These catalysts showed little selectivity to cinnamyl alcohol.

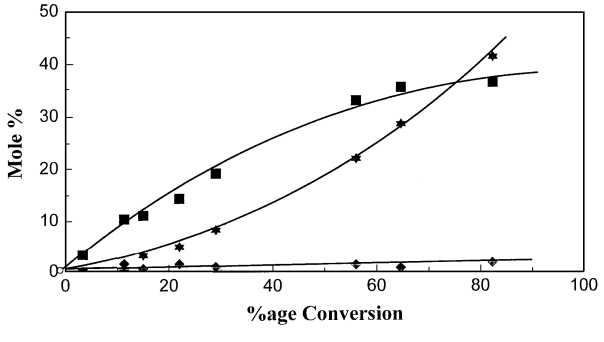

FIG. 4. Hydrogenation of cinnamaldehyde over reduced CuB/PQ: hydrocinnamaldehyde ■; cinnamyl alcohol ◆; phenyl propanol ★.

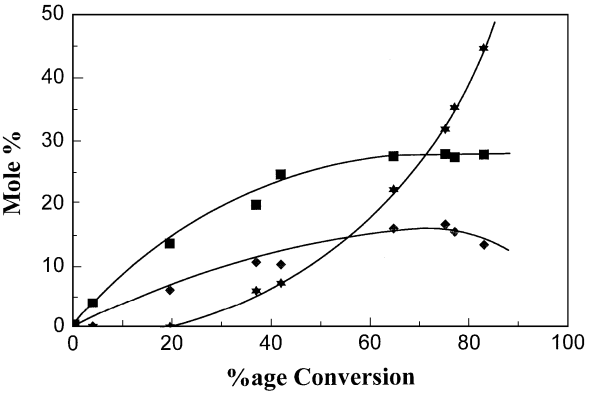

FIG. 5. Hydrogenation of cinnamaldehyde over reduced CuC/PQ: hydrocinnamaldehyde ■; cinnamyl alcohol ◆; phenyl propanol ★.

4. Reaction Mechanism

The results described above indicate that the hydrogenation of cinnamaldehyde is a sequential reaction, with phenyl propanol being formed by the hydrogenation of cinnamaldehyde to hydrocinnamaldehyde which is subsequently hydrogenated at ~20% conversion to give phenyl propanol. Only the reduced CuA/PQ catalyst showed significant selectivity to cinnamyl alcohol.

Two further experiments were carried out in order to gain more information on the mechanism of the selective hydrogenation of cinnamaldehyde. In the first of these, the hydrogenation of hydrocinnamaldehyde and cinnamyl alcohol was studied over redCuA/PQ using conditions identical to those used for the cinnamaldehyde hydrogenation and comparable concentrations of reagents. The hydrogenation of hydrocinnamaldehyde was found to be a zero-order reaction with a rate constant of 1.5×10^{-3} mol l^{-1} h^{-1}, i.e., the same as the rate obtained for cinnamaldehyde hydrogenation. The only product formed was phenyl propanol, indicating that the high selectivity to cinnamyl alcohol

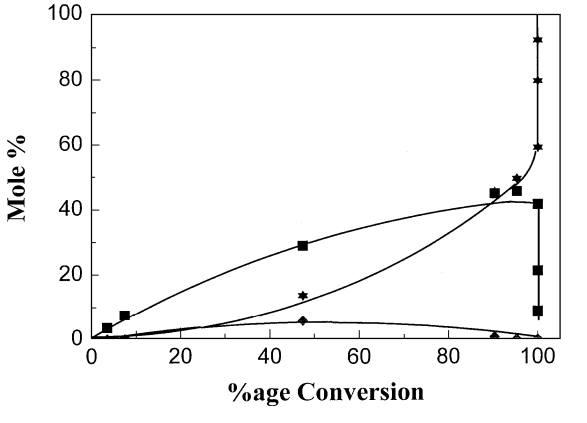

FIG. 6. Hydrogenation of cinnamaldehyde over reduced CuA/Pd1/PQ: hydrocinnamaldehyde ■; cinnamyl alcohol ◆; phenyl propanol ★.

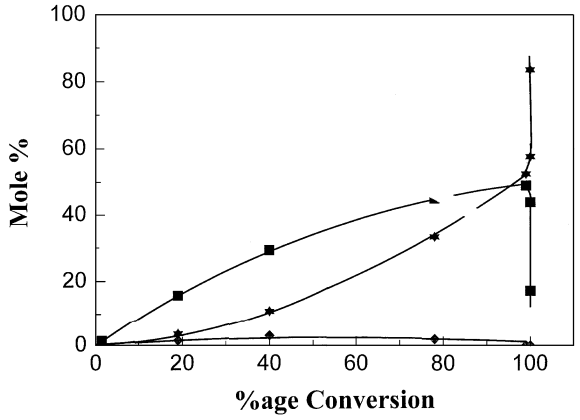

FIG. 7. Hydrogenation of cinnamaldehyde over reduced CuA/Grace: hydrocinnamaldehyde ■; cinnamyl alcohol ◆; phenyl propanol ★.

observed in the hydrogenation of cinnamaldehyde over this catalyst was due to hydrogenation of cinnamaldehyde rather than isomerisation of hydrocinnamaldehyde. The results for the reaction of cinnamyl alcohol with hydrogen are shown in Fig. 8. The conversion of cinnamyl alcohol was rapid, the rate being 24.3×10^{-3} mol l^{-1} h^{-1} and the reaction quickly deviated from zero-order kinetics. Figure 8 shows that, although hydrogenation of cinnamyl alcohol to phenyl propanol was the dominant pathway, hydrocinnamaldehyde was also formed, indicating that some of the cinnamyl alcohol was isomerised to hydrocinnamaldehyde. A result that is less readily explained is that some cinnamaldehyde was formed during the initial stages of the reaction, implying that dehydrogenation also occurred on the freshly reduced catalyst surface.

Further information on the reaction mechanism was obtained by reacting cinnamaldehyde with deuterium over calcined and reduced CuA/PQ following the procedure outlined in the experimental section. The extent of incorporation of deuterium in the cinnamaldehyde and reaction products was determined by proton and deuterium NMR

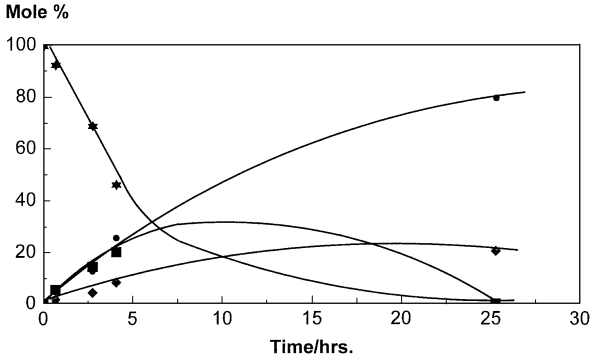

FIG. 8. Reaction of cinnamyl alcohol with hydrogen: hydrocinnamaldehyde ◆; cinnamyl alcohol ★; phenyl propanol ●; cinnamaldehyde ■.

spectroscopy. The deuterium spectrum showed three signals, whose intensities decreased consecutively, at $\delta = 1.898$, 2.763, and 3.697 ppm corresponding to deuterium situated on carbons 2, 3, and 1, respectively, of phenyl propanol. The different intensities of these three peaks confirm that the formation of phenyl propanol proceeds by a sequential mechanism via hydrocinnamaldehyde or cinnamyl alcohol intermediates. If this was not the case, the intensities of the peaks would all be equivalent, assuming that there was no deuterium–hydrogen exchange. Furthermore, if the only reactions taking place were the addition of deuterium across the carbon–carbon double bond in either the cinnamyl alcohol or the hydrocinnamaldehyde molecule, then the deuterium signals for carbons 2 and 3 would be expected to be the same. However, there was more deuterium on carbon 2 and this suggests that isomerisation occurs, in accordance with the results for the hydrogenation of cinnamyl alcohol. Two additional signals were observed at $\delta = 9.762$ and $\delta = 9.863$ ppm. The signal at $\delta = 9.863$ is further evidence for the isomerisation reaction since this signal can be ascribed to deuterium situated on the carbon of the carbonyl bond in hydrocinnamaldehyde. Assuming that no hydrogen–deuterium exchange occurs, this signal could only arise from isomerisation of the cinnamyl alcohol formed by deuteration of cinnamaldehyde. The isomerism route to deuterated hydrocinnamaldehyde is shown schematically in Fig. 9A. The signal at $\delta = 9.762$ is evidence for the dehydrogenation reaction, as this was assigned to deuterium on the carbon of the carbonyl bond in cinnamaldehyde. The dehydrogenation route to deuterated cinnamaldehyde is shown schematically in Fig. 9B.

DISCUSSION

These results clearly show that selectivity to cinnamyl alcohol in the hydrogenation of cinnamaldehyde is critically dependent on the way in which the catalyst is prepared. Catalysts redCuA/PQ and redCuB/PQ were prepared in different laboratories under similar conditions. New batches of each of the catalysts could be prepared reproducibly in each of the laboratories. Although the copper loadings were different (13.7 wt% for CuA/PQ and 12.4 wt% for CuB/PQ), it is unlikely that these differences were enough to explain the marked effect on the catalyst selectivity. Analysis of these samples by copper surface area measurements, TEM, TPR, and hot stage XRD did, however, reveal important differences between the two catalysts. Hot stage XRD studies showed that calCuA/PQ was not fully reduced after heating to 673 K in 4% H_2/N_2 and that reduction took place via the intermediate formation of Cu_2O. CalCuB/PQ, on the other hand, was fully reduced by 548 K after heating in 4% H_2/N_2 and no Cu_2O was detected during reduction. TPR studies confirmed that calCuA/PQ was more difficult to reduce

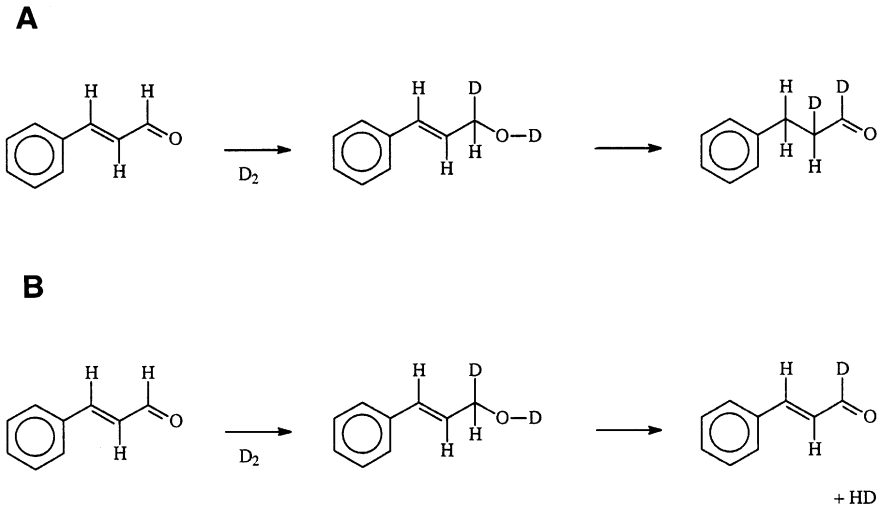

FIG. 9. Mechanistic scheme of the reaction of deuterium with cinnamaldehyde: (a) Formation of deuterated cinnamyl alcohol and isomerisation to deuterated hydrocinnamaldehyde; (b) dehydrogenation of deuterated cinnamyl alcohol.

than calCuB/PQ. A low temperature peak at 608 K and a high temperature peak at 628 K were present in equal amounts in calCuA/PQ, whereas the majority of the CuO was reduced at 603 K in calCuB/PQ. The copper area measured after reduction at 623 K was much lower for redCuA/PQ (0.08 $m^2\ g^{-1}$). Although TEM studies showed that both catalysts contained particles ranging from ~10 nm to ~250 nm, more smaller particles were present in redCuB/PQ. CuO and Cu particle sizes determined from X-ray line broadening studies showed that the CuO particles in calCuA/PQ were larger than those in calCuB/PQ and sintering occurred on reduction of calCuA/PQ to give copper crystallites ranging in size from 11 to 31.5 nm; sintering did not occur on reduction of calCuB/PQ and the copper crystallites were all ~21 nm.

These differences in the reducibility of the two catalysts may be ascribed to the differences in the particle sizes of the supported CuO. The support would then be functioning merely as a dispersing agent to facilitate the reduction of CuO, as suggested by Robertson *et al*. (16). The low and high temperature TPR peaks in calCuA/PQ would then correspond to the reduction of small and large CuO crystallites, respectively, the latter being more difficult to reduce on account of the slower rate of diffusion of hydrogen through the crystallites. Sintering would occur on reduction at the highest temperature resulting in the formation of some large copper crystallites. The predominance of the low temperature peak on reduction of calCuB/PQ would then correspond to the reduction of smaller CuO crystallites and sintering would not occur at this temperature. The smaller copper area for redCuA/PQ compared with redCuB/PQ would then be explained by the formation of larger copper crystallites in the former than the latter. Further, the TPR profile for calCuA/PQ that had been prepared by calcining the impregnated precursor at 623 K rather than the standard temperature of 723 K in flowing air; i.e., conditions which should result in the formation of smaller CuO particles due to less aggregation, showed that the reduction profile was shifted to lower temperatures. An additional peak emerged at 525 K and the copper area increased from 0.08 to 0.4 $m^2\ g^{-1}$. There was also better agreement between the actual and theoretical hydrogen consumptions after calcination at this lower temperature. However, it is difficult to explain the differences in theoretical and experimental hydrogen consumption observed for CuA/PQ after standard calcination procedures, the reduction via Cu_2O, and the low copper area on the basis of only particle size effects. Although low copper areas may be due to a predominance of low area copper particles, they are also characteristic of metal–support interactions (29). It is likely that there are some interactions of the smaller CuO crystallites with the support, possibly stabilising small amounts of Cu_2O at the metal–support interface following reduction. The presence of small amounts of unreduced copper have previously been reported for Cu/SiO_2 catalysts (21, 30) and attributed to metal–support interactions. Shimokawabe *et al*. (30) prepared Cu/SiO_2 catalysts by an ion-exchange route and found that their reducibility depended strongly on the conditions used in their preparation. Isolated Cu(II) ions which interacted weakly with the support were found to give peaks with maxima at 538 to 573 K and 673 K using 4% H_2/N_2 at 50 $cm^3\ min^{-1}$ and a heating rate of 10 K min^{-1}.

Addition of 200–5000 ppm of $Pd(NO_3)_2$ to $Cu(NO_3)_2 \cdot 3H_2O$/PQ followed by calcination in flowing air at 723 K resulted in a lowering of the reduction maxima for CuO in accordance with similar studies conducted by Gentry *et al*. (19), a separate low-temperature reduction for PdO

and an increase in the copper metal area. Since the low temperature peak corresponds to the complete reduction of PdO, the reduced palladium may provide a source of atomic hydrogen which spills over onto the CuO crystallites, providing a low energy pathway for the reduction of the CuO.

High selectivity to cinnamyl alcohol occurs preferentially when little free copper is available, i.e., at sites associated with metal oxide–support interactions and/or on large particles. Thus the low copper area redCuA/PQ catalyst was selective for cinnamyl alcohol, whereas redCuB/PQ, which had a much higher copper area, showed little selectivity for cinnamyl alcohol, even though the overall rate of reaction was similar for both catalysts. Hot stage XRD studies showed that calCuA/Grace was comprised of smaller CuO crystallites than calCuB/PQ, which had a similar CuO loading. TPR studies showed that calCuA/Grace was reduced to Cu in a single step with little or no interaction with the support. The rate of hydrogenation of cinnamaldehyde was much higher for redCuA/Grace than redCuB/PQ, in accordance with its smaller particle size and the absence of metal oxide–support interactions.

Both particle size effects and metal–support interactions have been shown to enhance the selective hydrogenation of unsaturated alcohols. Particle size effects were thought to arise from the phenyl group, sterically hindering the approach of the C=C moiety to the surface of a large particle (7, 10), leading to the preferential adsorption and subsequent hydrogenation of C=O to give the unsaturated alcohol and the facile desorption of the alcohol on larger crystallites (14). Strong metal–support interactions have been shown to enhance the reduction of crotonaldehyde to crotyl alcohol using poorly dispersed iridium and ruthenium on titania catalysts (31). The enhanced selectivity was ascribed to new catalytic sites which resulted from TiO_x decorating the supported metal particles after a high-temperature reduction treatment. Interactions with the support are likely to be much weaker in our case and are established at the calcination rather than the reduction stage, but they may still influence the selectivity to unsaturated alcohol. The metal oxide–support interactions may stabilise small amounts of Cu_2O at the metal–support interface following reduction. Copper(I) has been proposed as an active site in selective hydrogenation reactions. Fragale *et al*. (32) studied the hydrogenation of polyenes over supported copper catalysts. They attributed the selective hydrogenation of an isolated olefinic bond to the presence of a small amount of Cu(I) present in the reduced catalyst surface. The Cu(I) was thought to promote isomerisation of the isolated double bond to a conjugated position so that it could be subsequently hydrogenated by Cu(0). The importance of Cu(I) in the selective hydrogenation of conjugated unsaturated aldehydes has been established previously for copper chromite catalysts (3). The active site for hydrogenation in this catalyst was thought to be an octahedrally coordinated Cu^+ ion with two anionic vacancies and an attached hydride ion (H^-). Low selectivity for unsaturated alcohol was attained in this case since the Cr^{3+} in the support catalysed the isomerisation and dehydroxylation of the adsorbed allyl alcohol. Isomerisation is unlikely to occur in our case using a silica support.

The main role of palladium added to redCuA/PQ was to increase the rate of hydrogenation by dispersing the CuO to give smaller crystallites which did not sinter appreciably during reduction and catalysis. The hydrogenation of cinnamaldehyde to hydrocinnamaldehyde seemed to take place preferentially on smaller crystallites so that the rate increases with increasing copper area.

RedCuB/V/PQ, like redCuB/PQ, was not selective for the 1,2-hydrogenation of cinnamaldehyde to cinnamyl alcohol. TPR studies showed that V_2O_5 and CuO were reduced concomitantly with partial reduction of V(V) to V(IV). It was thought that copper–vanadia bronze might form and provide a means of storing and releasing hydrogen, but if so it appeared to retain the hydrogen too strongly. Indeed, the rate of reaction was exceedingly slow. Addition of palladium to CuB/V/PQ accelerated the rate of hydrogenation (Table 4), far exceeding that expected from the small increase in copper surface area (Table 3). The negligible rate of hydrogenation in the absence of palladium and appearance of a second reduction peak in the TPR profile for this sample suggests that the hydrogenation takes place on the palladium sites rather than the "modified" copper in this case.

A more detailed description of the reaction mechanism of hydrogenation (11) (Fig. 2) can now be formulated. Our results indicate that in the sequential reaction phenyl propanol is formed by the successive hydrogenation of cinnamaldehyde and hydrocinnamaldehyde over the supported copper catalysts described in this paper, since it did not appear until ~20% of the cinnamaldehyde had been hydrogenated. Cinnamaldehyde was hydrogenated exclusively to hydrocinnamaldehyde during the initial stages of the reaction for each of the catalysts studied, suggesting that the catalyst surface is modified by hydrocinnamaldehyde before reaction to give cinnamyl alcohol and phenyl propanol can occur. This effect has been observed previously for cinnamaldehyde hydrogenation using supported iridium, platinum, ruthenium, and rhodium catalysts (6, 10, 12). Following the initial hydrogenation, hydrocinnamaldehyde desorbs from the modified surface and further hydrogenation yields phenyl propanol and, in some cases, cinnamyl alcohol as reaction products. Some of the cinnamyl alcohol is isomerised to hydrocinnamaldehyde as the reaction proceeds. Evidence for the isomerization route is provided by the fact that the reaction of cinnamyl alcohol with hydrogen resulted in some hydrocinnamaldehyde and studies in which cinnamaldehyde was reacted with deuterium

showed that deuterium was incorporated on the carbon of the carbonyl bond in hydrocinnamaldehyde. However, redCuA/PQ retains its high selectivity to cinnamyl alcohol, even at very high conversions, indicating that the rapid hydrogenation of cinnamyl alcohol to phenyl propanol observed in the separately studied reaction of cinnamyl alcohol with hydrogen over redCuA/PQ (Fig. 8) is suppressed when the surface has been modified during a preceding cinnamaldehyde hydrogenation over this catalyst.

CONCLUSIONS

1. The hydrogenation of cinnamaldehyde can readily be carried out using silica-supported copper catalysts. High selectivity to cinnamyl alcohol can be attained by optimising preparative conditions to give large particles and/or metal oxide–support interactions.

2. Palladium accelerates the rate of cinnamaldehyde hydrogenation, but selectivity to cinnamyl alcohol is lost.

3. Phenyl propanol is formed predominantly by the consecutive hydrogenation of cinnamaldehyde and hydrocinnamaldehyde.

ACKNOWLEDGMENTS

Support from both EPSRC and ICI Katalco for this work is gratefully acknowledged.

REFERENCES

1. Isagulyants, V. I., "Synthetic Fragrances," *Izv. Akad. Nauk Armenii SSR, Yerevan* (1947).
2. Jenck, J., and Germain, J. E., *J. Catal.* **65**, 141 (1980).
3. Hubaut, R., Bonnelle, J. P., and Daage, M., *J. Mol. Catal.* **55**, 170 (1989).
4. Hubaut, R., Daage, M., and Bonnelle, J. P., *Appl. Catal.* **22**, 231 (1986).
5. Rylander, P., *in* "Catalytic Hydrogenation over Platinum Metals," Academic Press, New York, 1967.
6. Giroir-Fendler, A., Richard, D., and Gallezot, P., *in* "Heterogeneous Catalysis and Fine Chemicals" (M. Guisnet, J. Barrault, C. Bouchoule, D. Duprez, C. Montassier, and G. Perot, Eds.), p. 171, Elsevier, Amsterdam, 1988.
7. Galvagno, S., Capannelli, G., Neri, G., Donato, A., and Pietropado, R., *J. Mol. Catal.* **64**, 237 (1991).
8. Nitta, Y., Hiramatsu, Y., and Imanaka, T., *J. Catal.* **126**, 235 (1990).
9. Rylander, P. N., and Steele, D. R., *Engelhard Ind. Tech. Bull.* **10**, 17 (1969).
10. Richard, D., Fouilloux, P., and Gallezot, P., "Proc. 9th Int. Cong. Catal., Calgary, 1988" (M. J. Phillips and M. Ternan, Eds.), p. 1074, Chem. Inst. Canada, Ottawa, 1988.
11. Galvagno, S., Donato, A., Neri, G., Pietropaolo, R., and Pietropaolo, D., *J. Mol. Catal.* **49**, 223 (1989).
12. Marinelli, T. B. L. W., Vleeming, J. H., and Ponec, V., "Proc. 10th int. Cong. Catal., Budapest, 1992" (L. Guczi, F. Solymosi, and P. Tétényi, Eds.), p. 1211, Akademiai Kiado, Budapest, 1993.
13. Galvagno, S., Donato, A., Neri, G., Pietropaolo, R., and Capannelli, G., *J. Mol. Catal.* **78**, 227 (1993).
14. Nitta, Y., Ueno, K., and Imanaka, T., *Appl. Catal.* **56**, 9 (1989).
15. Duffy, J. A., "Bonding, Energy Levels and Bands in Inorganic Solids," Wiley, London, 1990.
16. Robertson, S. D., McNicol, B. D., Baas, J. H., Kloet, S. C., and Jenkins, J. W., *J. Catal.* **37**, 424 (1975).
17. Chinchen, G. C., Hay, C. M., Vandervell, H. D., and Waugh, K. C., *J. Catal.* **103**, 79 (1987).
18. West, A. R., "Solid State Chemistry and its Applications," p. 174, Wiley, Chichester, 1985.
19. Gentry, S. J., Hurst, N. W., and Jones, A., *J. Chem. Soc. Faraday I* **77**, 603 (1981).
20. Stirling, D., Ph.D. thesis, Liverpool Polytechnic, 1985.
21. Delk, F. S., and Vavere, A., *J. Catal.* **85**, 380 (1984).
22. Jones, A., and McNicol, B. D., "Temperature-Programmed Reduction for Solid Materials Characterisation," Dekker, New York, 1986.
23. Roozeboom, F., Mittelmeijer-Hazelleger, M. C., Moulijn, J. A., Medema, J., de Beer, V. H. J., and Gellings, P. J., *J. Phys. Chem.* **84**, 2738 (1980).
24. Bosch, H., Kip, B. J., van Ommen, J. G., and Gellings, P. J., *J. Chem. Soc. Faraday Trans. I* **80**, 2479 (1984).
25. Bond, G. C., Zurita, J. P., Flamerz, S., Gellings, P. J., Bosch, H., van Ommen, J. G., and Kip, B. J., *Appl. Catal.* **22**, 361 (1986).
26. van Hengstum, A. J., van Ommen, J. G., Bosch, H., and Gellings, P. J., "Proc. 8th Int. Cong. Catal., Berlin 1984," Vol. IV, p. 297, Verlag Chemie, Weinheim, 1984.
27. Iwamoto, M., Takenaka, T., Matsukami, K., Hirata, J., Kagawa, S., and Izumi, J., *Appl. Catal* **16**, 153 (1985).
28. Khoobiar, S., *J. Phys. Chem.* **68**, 411 (1964).
29. Chen, H., White, J. M., and Ekerdt, J. G., *J. Catal.* **99**, 293 (1986).
30. Shimokawabe, M., Takezawa, N., and Kobayashi, H., *Bull. Chem. Soc., Japan* **56**, 1337 (1983).
31. Kašpar, J., Graziani, M., Escobar, G. P., and Trovarelli, A., *J. Mol. Catal.* **72**, 243 (1992).
32. Fragale, C., Gargano, M., and Rossi, M., *J. Amer. Oil Chem. Soc.* **59**, 465 (1982).